Operation and Control Strategy of a New Hybrid ESS-UPS System

Sangjin Kim, Minho Kwon, and Sewan Choi, *Member, IEEE*

***Abstract*—This paper proposes a hybrid energy storage system (ESS) that integrates an ESS with an online uninterruptible power supply (UPS). The power conversion system cost of the proposed hybrid ESS-UPS is reduced, and battery utilization is increased by using the energy of the integrated battery for both demand management and emergency power supply. Further, unlike the conventional online UPS, the proposed hybrid ESS-UPS is capable of supplying emergency power to two types of critical loads, voltage-frequency independent (VFI) load and voltage-frequency dependent (VFD) load. A seamless mode transfer algorithm of the ac–dc converter is proposed for supplying uninterruptible power to the VFD load as well. In addition, an autonomous and seamless mode transfer algorithm of the bidirectional dc–dc converter is proposed to minimize the transient across the dc link that could affect the power quality of the VFD load and the VFI load at the mode transition. To validate the proposed control scheme, experimental results from a 5-kW prototype are provided.**

***Index Terms*—Energy storage system (ESS), hybrid ESS, seamless mode transfer, uninterruptible power supply (UPS).**

I. Introduction

ENERGY storage systems (ESSs) have attracted attention as a way to avoid massive power outages resulting from a sudden increase of power usage in summer and winter [1]–[6]. The ESSs can be used to address power quality issues by providing ancillary services such as peak shaving, load shifting, etc., to the grid [7]–[20]. In the meantime, uninterruptible power supply (UPS) systems have been widely used in datacenters, hospitals, etc., to provide reliable power to critical loads such as communication systems, network servers, medical equipment, etc. Fig. 1 shows a conventional configuration that includes an ESS for demand management and an online UPS for emergency power supply, where the stored energy of the ESS battery is used for demand management, but the stored energy of the UPS battery is used only when the grid fails [21]–[25]. Further, when the grid fails, the ac–dc rectifier of the online UPS stops its operation and the dc–ac inverter keeps supplying the emergency power only to the VFI load.

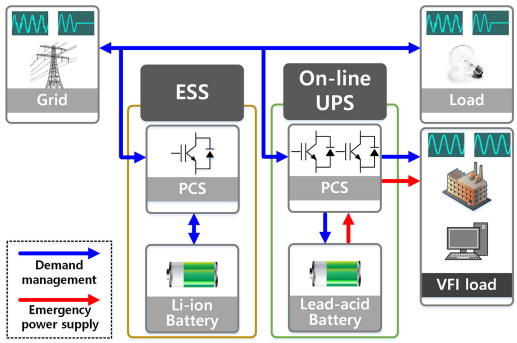

Fig. 1. Configuration of the conventional ESS and UPS.

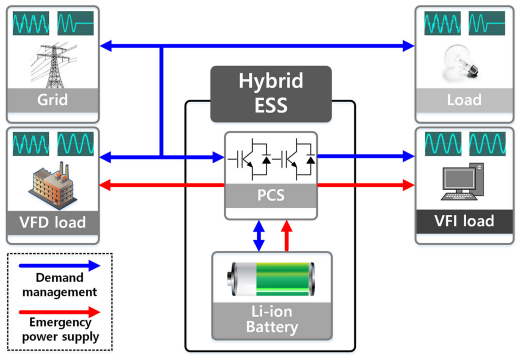

Fig. 2. Configuration of the proposed hybrid ESS-UPS.

In this study, a hybrid ESS-UPS is proposed not only for efficient use of battery energy and cost reduction of the power conversion system (PCS) by integrating the ESS with the UPS, but also for increased capacity of emergency power by supplying an additional voltage-frequency dependent (VFD) load. Fig. 2 shows the configuration of the proposed hybrid ESS-UPS. When the grid is under normal operation, the proposed hybrid ESS-UPS performs charging or discharging of the integrated battery for demand management, thereby acting like an ESS, whereas when the grid fails, the system supplies emergency power to VFD and/or VFI loads, thereby acting like a UPS. The VFD and the voltage-frequency independent (VFI) loads are critical loads according to international UPS classification by IEC 62040-3 [26]. The proposed hybrid ESS requires repeated battery charge and discharge operations for demand management. Since the frequent cycling of the battery will shorten the lifetime of the battery, the Li-ion battery is selected for the proposed system.

Manuscript received January 16, 2017; revised April 3, 2017 and June 5, 2017; accepted July 11, 2017. Date of publication July 28, 2017; date of current version February 22, 2018. This work was supported by the Korea Institute of Energy Technology Evaluation and Planning (KETEP) and the Ministry of Trade, Industry & Energy(MOTIE) of the Republic of Korea (No. 20142010102600). Recommended for publication by Associate Editor G. Oriti. *(Correspondence author: Sewan Choi.)*

The authors are with the Department of Electrical and Information Engineering, Seoul National University of Science and Technology, Seoul 139-743, South Korea (e-mail: winston88@seoultech.ac.kr; saemnae@seoultech.ac.kr; schoi@seoultech.ac.kr).

Color versions of one or more of the figures in this paper are available online at http://ieeexplore.ieee.org.

Digital Object Identifier 10.1109/TPEL.2017.2733019

TABLE I
COMPARISON BETWEEN THE CONVENTIONAL ONLINE UPS, THE CONVENTIONAL ESS AND THE PROPOSED HYBRID ESS-UPS

Function of the system	Conventional on-line UPS	Conventional ESS	Proposed Hybrid ESS-UPS
Uninterruptible power supply for VFI load	O	X	O
Uninterruptible power supply for VFD load	X	X	O
Demand management	X	O	O
Reactive power compensation	X	O	O

TABLE II
COST COMPARISON BETWEEN THE CONVENTIONAL SEPARATE ESS-UPS AND THE PROPOSED HYBRID ESS-UPS

	Conventional separate ESS-UPS		Proposed Hybrid ESS-UPS
	On-line UPS	PCS of ESS	
Rated power	250 kW	250 kW	250 kW
Cost	$ 44,970	$ 40,321	$ 52,429
Sum	$ 85,291		$ 52,429

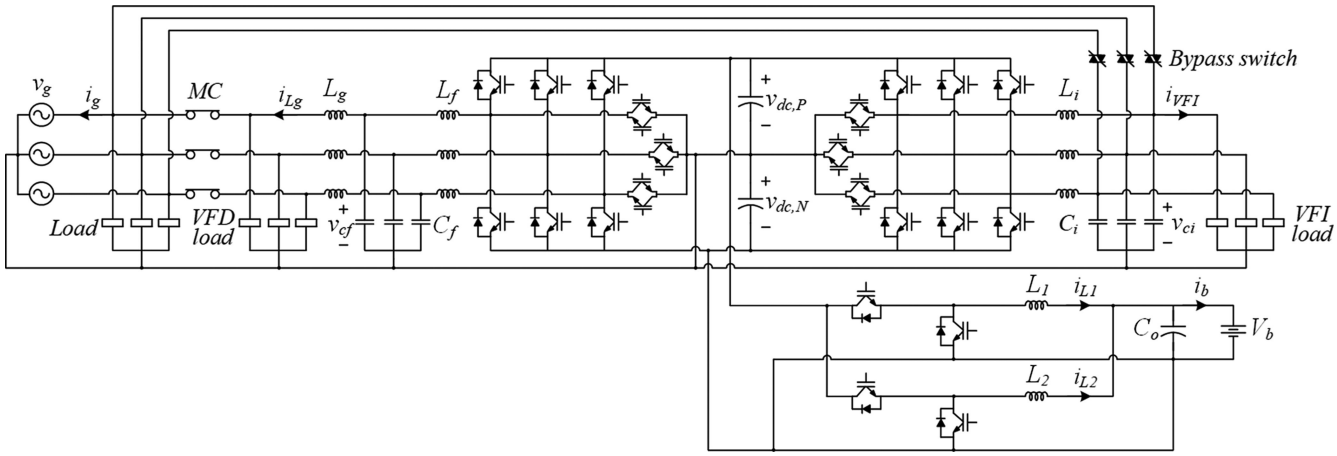

Fig. 3. Circuit diagram of the proposed hybrid ESS-UPS.

Although the Li-ion battery is more expensive than the lead-acid battery, the Li-ion battery could be more economical in the long term than the lead-acid battery due to the following two reasons [27], [28]: 1) the Li-ion battery has two times longer calendar life than the lead-acid battery due to its long lifetime feature, thereby saving costly replacement labor; 2) the volumetric energy density of the Li-ion battery is 2.5 times higher than the lead-acid battery, thereby reducing system weight and footprint.

Table I summarizes the comparison between the conventional online UPS, the conventional ESS, and the proposed hybrid ESS-UPS. The conventional online UPS is able to provide uninterruptible power only for VFI load. The conventional ESS provides functions of the demand management and reactive power compensation, but the stored battery energy is used to supply the emergency power to the critical load. On the other hand, the proposed hybrid ESS-UPS is able to provide all of the above functions. Table II represents the cost comparison between the conventional separate ESS-UPS and the proposed hybrid ESS-UPS. The PCS cost of the hybrid ESS-UPS is reduced by 38.5% compared to the conventional separate ESS-UPS. The cost of PCS was estimated with the help of a UPS company in South Korea named "KUKJE Electric Manufacture Co."

In order to realize the proposed hybrid ESS-UPS, this paper proposes a hybrid ESS-UPS configuration that is capable of supplying not only the VFI load but also the VFD load and a seamless mode transfer algorithm of the ac–dc converter for supplying uninterruptible power to the VFD load as well. In addition, an autonomous and seamless mode transfer algorithm of the bidirectional dc–dc converter is proposed to minimize the transient across the dc link that may affect the power quality of the VFD load and the VFI load at the mode transition. With the proposed hybrid ESS-UPS configuration and mode transfer algorithms, the proposed hybrid ESS-UPS has the following advantages:

1) increased capacity of emergency power supply, that is, supplying the VFD load as well as the VFI load when the grid fails, unlike the conventional online UPS that supplies only the VFI load;
2) cost reduction by integrating the PCS of the ESS with that of the UPS;
3) increased battery utilization by using the energy of the integrated battery for both demand management and emergency power supply.

In order to achieve the advantages mentioned earlier, this study proposes the circuit topology of the integrated PCS, the operation modes, and the control strategy of the proposed hybrid ESS-UPS. Also, a fast and smooth mode transfer algorithm is proposed to minimize the transient caused by switchover between demand management and emergency power supply modes. In order to validate performance of the proposed algorithm experimental, results from a 5-kW prototype are provided.

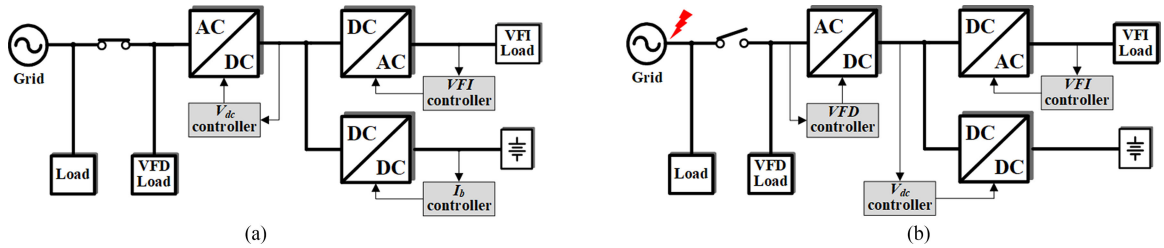

Fig. 4. Control objectives of the proposed hybrid ESS-UPS. (a) Demand management mode. (b) Emergency power supply mode.

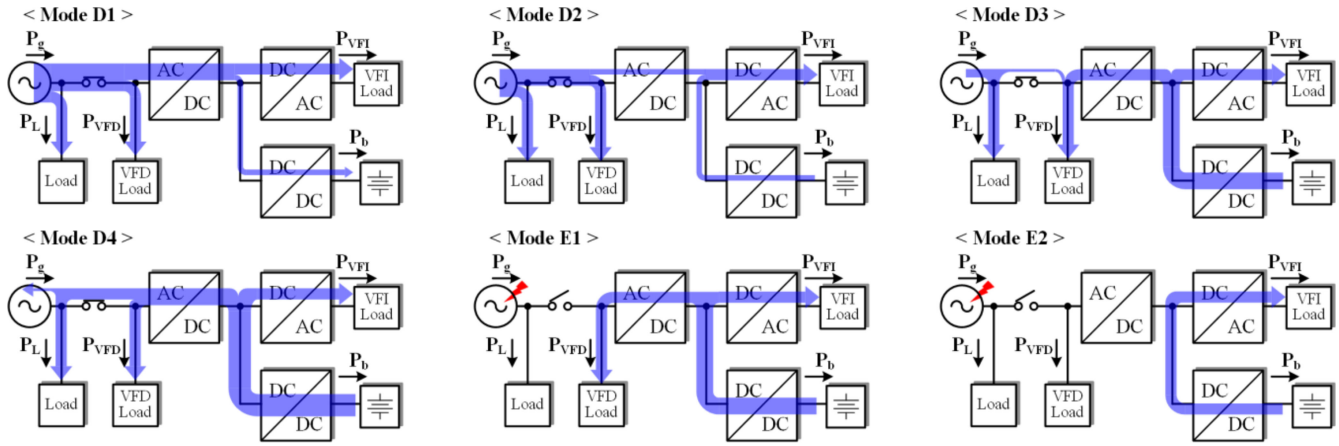

Fig. 5. Operation modes of the proposed hybrid ESS-UPS. (a) Mode D1. (b) Mode D2. (c) Mode D3. (d) Mode D4. (e) Mode E1. (f) Mode D2.

II. Proposed Hybrid ESS-UPS

Fig. 3 shows the circuit diagram of the proposed hybrid ESS-UPS that is based on a double conversion structure of UPS. Recently, it has been reported that UPSs based on a double conversion structure achieve high power conversion efficiency using three-level topology [29]. In this study, the three-level T-type topology is adopted to reduce the filter size and achieve high power conversion efficiency. The proposed system has two types of critical loads. One is the VFI load that is connected to the output of the dc–ac inverter, and the other is the VFD load that is connected to the main grid side.

In this paper, the proposed system is assumed to combine a 250-kW ESS that has demand management function and a 250-kW UPS that has the emergency power supply function in one unit. Then, the rated powers of the VFD and VFI loads of the proposed system become 250 kW, respectively, and the battery storage capacity of the proposed system becomes 500 kWh that is the same as sum of the battery capacities of the conventional ESS and UPS shown in Fig. 1. Therefore, both the ac-dc converter and the dc-ac inverter are rated at 250-kW.

When the grid is normal, the proposed system operates either in the battery charging mode or in the demand management mode according to the power demand and the battery SOC. In the battery charging mode, the grid could not only supply the VFI load through the ac–dc converter and the dc–ac inverter, but also charge the battery through the ac–dc converter and the dc–dc converter. Therefore, sum of the VFI load power and the battery charging power should be limited to 250 kW in the battery charging mode. In the demand management mode, the dc–dc converter discharges the battery to supply not only the VFI load through the dc–ac inverter, but also the VFD load and the grid through the ac–dc converter. Therefore, sum of the VFD load power and injected power to the grid is limited to 250 kW, and a dc-dc converter is rated at 250-kW. It is obvious that the maximum discharge power of the battery is 500 kW that is sum of the rated powers of the VFI and VFD load.

TABLE III
Power Flow Under Different Operation Modes

Operation Modes	Power	
	Grid	Battery
Mode D1	$P_g > P_L+P_{VFD}+P_{VFI}$	$P_b > 0$
Mode D2	$P_g > P_L+P_{VFD}$	$0 < \lvert P_b \rvert < P_{VFI}$, $P_b < 0$
Mode D3	$P_L < P_g < P_{VFD}$	$P_{VFI} < \lvert P_b \rvert < P_{VFI}+P_{VFD}$, $P_b < 0$
Mode D4	$P_g < 0$	$\lvert P_b \rvert > P_L+P_{VFD}+P_{VFI}$, $P_b < 0$
Mode E1	$P_g = 0$	$\lvert P_b \rvert = P_{VFD}+P_{VFI}$, $P_b < 0$
Mode E2	$P_g = 0$	$\lvert P_b \rvert = P_{VFI}$, $P_b < 0$

A. Control Strategy and Operating Modes

Fig. 4 shows the control objective of each of the converter according to the operation mode. When the ac input voltage is within the preset tolerance, the proposed system operates in the demand management mode, as shown in Fig. 4(a), where the

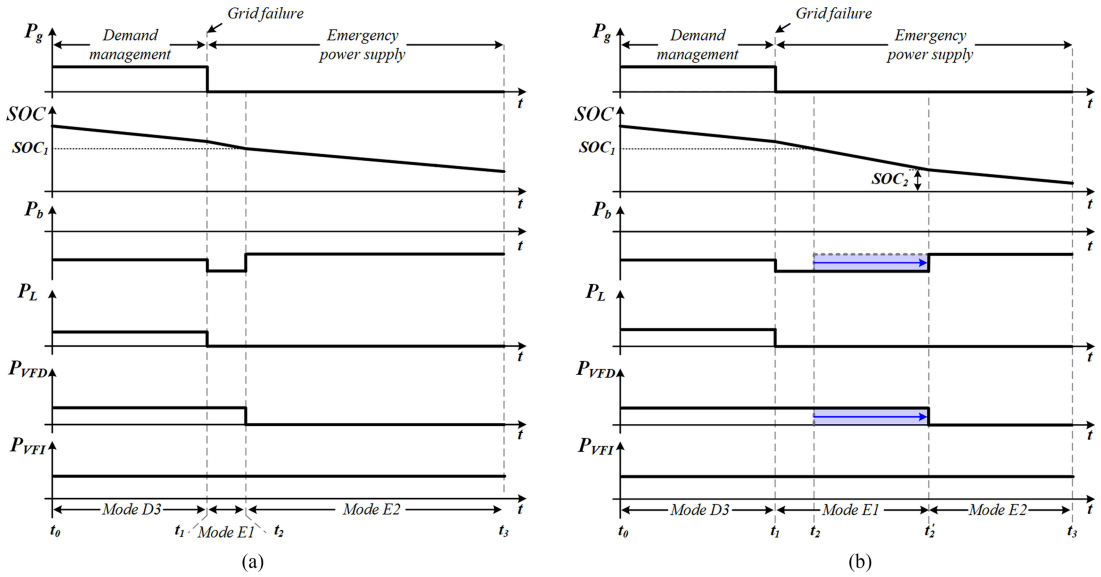

Fig. 6. Power flows of the proposed hybrid ESS-UPS during the mode transfer: (a) without demand forecasting and (b) with demand forecasting.

ac–dc converter regulates the dc-link voltage while the dc–ac inverter supplies well-regulated three-phase voltage for the VFI load. The dc–dc converter performs charging or discharging with the reference battery current determined by the energy management system (EMS). In the event of a grid fault, the system operates in the emergency power supply mode, as shown in Fig. 4(b), where the magnetic contactor (MC) disconnects the ac–dc converter from the grid, and the ac–dc converter changes its control objective from the dc-link voltage to the VFD load voltage. At the same time, the control objective of the dc–dc converter is also changed from battery current to dc-link voltage. In order to achieve good dynamic performance, the transient at the mode change should be minimized.

The demand management mode and the emergency power supply mode can further be divided into four modes of D1, D2, D3, and D4, and two modes of E1 and E2, respectively, as shown in Fig. 5, according to grid status and amount of battery charging or discharging power P_b. Mode D1 represents the battery charging mode. When the power consumption is low, usually at night, the system accumulates energy into the battery. In Mode D2, Mode D3, and Mode D4, the dc–dc converter performs battery discharging for demand management. Mode D2 shows that the VFI load power is provided from the grid and the battery because the battery discharging power is smaller than the required VFI load power. During Mode D3, the VFD load power is supplied from the grid and the battery because the battery discharging power is larger than the required VFI load power. In Mode D4, the battery discharging power is larger than the sum of the VFD load power and the VFI load power. Therefore, the battery discharging power flows from the battery to the grid. When the grid fails, the MC disconnects the system from the grid and the system enters into Mode E1, where the dc–dc converter discharges the battery in order to supply emergency power to the VFI load and the VFD load. When the battery state-of-charge (SOC) reaches down to SOC_1, which is defined as the battery SOC for supplying emergency power to a rated VFI load for 30 min during Mode E1, the system enters into Mode E2. In Mode E2, the system supplies emergency power only to the VFI load and, at the same time, stops providing emergency power to the VFD load. The power flows of the proposed hybrid ESS-UPS are listed in Table III, where the positive directions of power flows are defined in Fig. 5.

Fig. 6 shows the power flows when the system transfers from the demand management mode to emergency power supply mode. In this study, SOC_2 is defined as the battery SOC for supplying emergency power to a rated VFI load and estimated by demand forecasting of the EMS. The demand forecasting is done based on load-profile data accumulated during system operation, and the amounts of VFI and VFD load power before grid failure. Grid power P_g is determined by the sum of battery power P_b, load power P_L, VFD load power P_{VFD}, and VFI load power P_{VFI} as follows:

$$P_g = P_b + P_L + P_{\mathrm{VFD}} + P_{\mathrm{VFI}}. \tag{1}$$

Fig. 6(a) and (b) shows that the system transfers from Mode D3 to Mode E1 when the grid fails at t_1. At t_1, the amount of battery discharging power is determined as follows:

$$P_b = -(P_{\mathrm{VFD}} + P_{\mathrm{VFI}}). \tag{2}$$

When the battery SOC reaches down to SOC_1, the system stops supplying power to the VFD load but keeps supplying emergency power only to the VFI load if the system does not have demand forecasting, as shown in Fig. 6(a). On the other hand, Fig. 6(b) shows that the system stops supplying power to the VFD load but keeps supplying emergency power only to the VFI load when the battery SOC reaches down to SOC_2 (not SOC_1) since the system has been operating based on the data from demand forecasting of the EMS. With demand forecasting, the system is able to extend the length of time it

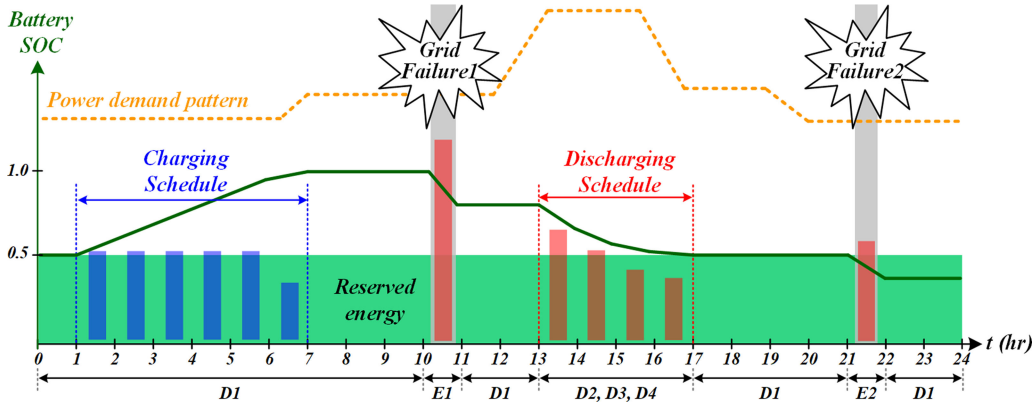

Fig. 7. Operation scenario of the proposed hybrid ESS-UPS according to power demand pattern and battery SOC.

supplies emergency power to the VFD load, resulting in more efficient use of battery power.

Fig. 7 shows the operation scenario of the proposed hybrid ESS-UPS according to a power demand pattern and battery SOC. The power demand pattern is obtained by demand forecasting performed by EMS. The charging and discharging is also scheduled by EMS considering the power demand pattern to manage battery SOC. Reserved energy stored in the battery represents the capacity of the backup power that is supposed to supply the VFI load during the backup battery runtime determined by the user.

As shown in Fig. 7, the proposed system basically operates according to the predefined schedule of charging the battery during the light load hours with low electricity rates and discharging the battery for demand management during the heavy load hours with high electricity rates. In this paper, the 250-kW hybrid ESS-UPS that integrates the 250-kW ESS with the 250-kW UPS was proposed. Therefore, half of the energy stored in the proposed system is basically used for the demand management and the rest of the energy (reserved energy for UPS) is used for the emergency power supply. The amount of the reserved energy can be varied by the demand forecasting of the EMS. When the grid fails, the proposed system goes into Mode E1 or Mode E2 according to the battery SOC. In case of the Grid Failure 1, where the battery SOC is high enough, the proposed system operates in Mode E1. On the other hand, in case of the Grid Failure 2, where the battery SOC is low, the proposed system operates in Mode E2.

III. Control Strategy of Hybrid ESS-UPS for Seamless Mode Change

The proposed hybrid ESS-UPS should supply emergency power to the VFD load as well as the VFI load when the grid fails. In order to supply emergency power to the VFD load, it is required for the ac–dc converter to switch the control objective from the dc-link voltage to the VFD load voltage while the dc–dc converter switches the control target from the battery current to the dc-link voltage. The switchover of the control objective may cause large transients across the VFD load and dc link, and therefore, fast and smooth mode transfer algorithms are required for both the ac–dc converter and the dc–dc converter.

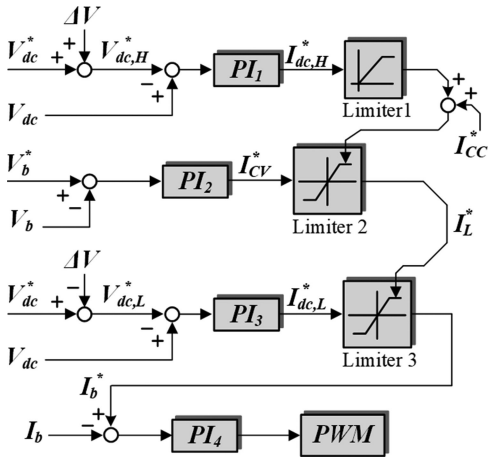

Fig. 8. Proposed control block diagram of the bidirectional dc–dc converter.

A. Control of Bidirectional DC–DC Converter

Fig. 8 shows the proposed control block diagram of the bidirectional dc–dc converter for autonomous and seamless mode transfer [30]–[32]. The proposed autonomous and seamless mode transfer algorithm is based on the variable limiter technique and the dc-bus signaling that is a means of communication of utilizing the dc-bus as the communication link [33], [34]. The proposed algorithm is composed of three parts: two voltage controllers PI_1 and PI_3 for regulating the dc-link voltage at the occurrence of a grid failure, a battery voltage controller PI_2 for constant voltage charging after the battery voltage reaches the final discharge voltage, and a current controller PI_4 for charging or discharging the battery. Each of the voltage controllers is saturated or activated according to the grid status, and when the saturated controllers are activated, the windup of the controllers caused by accumulated error in the integrator may occur. Thus, the antiwindup technique is implemented to prevent windup of the controller during mode transfer [35].

References $V_{dc+}{}^*$ and $V_{dc-}{}^*$ of the dc-link voltage controllers PI_1 and PI_3 are determined, respectively, as follows:

$$V^*_{dc+} = V^*_{dc} + \Delta V \tag{3}$$

$$V^*_{dc-} = V^*_{dc} - \Delta V \tag{4}$$

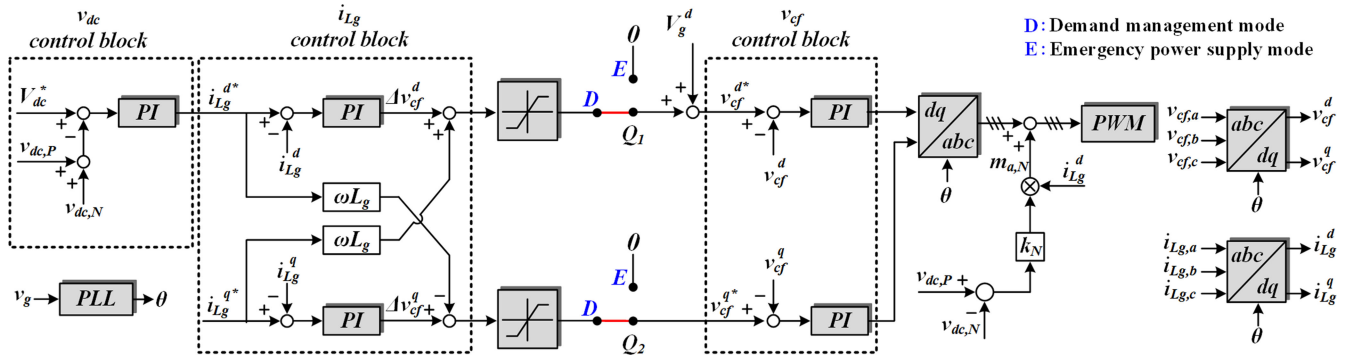

Fig. 9. Proposed control block diagram of the three-level ac–dc converter.

where $V_{\rm dc}^*$ is the same as the nominal dc-link voltage regulated by the ac–dc converter, and ΔV represents an allowable range of the dc-link voltage fluctuation caused by disturbance. Only when the dc-link voltage goes down below $V_{\rm dc}^* - \Delta V$ or goes up over $V_{\rm dc}^* + \Delta V$ due to a fluctuation, the dc–dc converter is supposed to switch the control objective from battery current to dc-link voltage. In order to avoid unwanted change of the control objective by the disturbance, ΔV should properly be designed considering the worst case fluctuation plus margin. In this paper, ΔV is set to 5% of $V_{\rm dc}^*$. Battery voltage reference V_b^* is set to the final discharge voltage of the battery. $I_{\rm CC}^*$ represents the battery current reference that comes from the EMS during the constant current (CC) mode (Mode D1) or during the demand management mode (Mode D2, D3, and D4). When the grid is normal, dc-link voltage $V_{\rm dc}$ is regulated to $V_{\rm dc}^*$ by the ac–dc converter, which leads to saturations of controller $\rm PI_1$ to a negative value causing Limiter 1 to output zero and controller $\rm PI_3$ to a positive value causing Limiter 3 to output I_L^*. In a similar way, assuming that the battery voltage did not reach to V_b^* yet, controller $\rm PI_2$ is also saturated to a positive value, thereby causing Limiter 2 to output $I_{\rm CC}^*$. Therefore, the battery current reference i_b^* becomes

$$I_b^* = I_L^* = I_{\rm CC}^*. \tag{5}$$

Therefore, the bidirectional dc–dc converter charges the battery with CC $I_{\rm CC}^*$ until the battery is fully charged. When V_b reaches the final discharge voltage of the battery, $\rm PI_2$ is activated and starts to regulate V_b to constant voltage V_b^*. In order to regulate V_b to V_b^*, charging current I_b^* is determined as follows:

$$I_b^* = I_L^* = I_{CV}^*. \tag{6}$$

When the grid fails during battery charging, the dc-link voltage starts to decrease, and the mode is changed from demand management mode to emergency power supply mode. The bidirectional dc–dc converter should switch the control objective from the battery current or battery voltage to the dc-link voltage and start to regulate the dc-link voltage instead of the ac–dc converter. A decrease of the dc-link voltage activates $\rm PI_3$, and its output I_b^* becomes ${I_{{\rm dc},L}}^*$ in order to regulate the dc-link voltage. ${I_{{\rm dc},L}}^*$ is a current reference to regulate the dc-link voltage, and $V_{\rm dc}$ is regulated by $\rm PI_3$ as follows:

$$V_{\rm dc} = V_{\rm dc}^* - \Delta V. \tag{7}$$

On the other hand, when the grid fails during the battery discharging, $\rm PI_1$ is activated since $V_{\rm dc}$ starts to increase. The output of $\rm PI_1$, ${I_{{\rm dc},H}}^*$, becomes the current reference to regulate $V_{\rm dc}$ to ${V_{\rm dc}}^* + \Delta V$ and I_b^* is determined by ${I_{\rm CC}}^* + {I_{{\rm dc},H}}^*$. Therefore, the dc–dc converter can autonomously change the mode from the battery current control mode to the dc-link voltage control mode by variation of the dc-link voltage.

B. Control of Three-Level AC–DC Converter

Fig. 9 shows the proposed control block diagram of the three-level ac–dc converter for seamless mode transfer [36]–[38]. It consists of the dc-link voltage controller, the grid-side current controllers, and the capacitor voltage controllers. In the demand management mode, the mode control switches Q_1 and Q_2 are connected to "D," and the ac–dc converter regulates the dc-link voltage by controlling the grid-side current. Note that the PI controllers of the v_{cf} control block are used to control the grid-side current. When the grid fails, the mode control switches Q_1 and Q_2 are connected to "E," and the ac–dc converter goes into the emergency power supply mode. The PI controllers of the v_{cf} control block are still activated, although the control target is switched from the dc-link voltage to the capacitor voltage, resulting in negligible transient across the VFD load.

In demand management mode, the relation of grid-side inductor voltage v_{Lg}, grid voltage V_g, capacitor voltage reference v_{cf}^*, and grid-side inductor current reference I_{Lg}^* can be expressed as follows:

$$v_{Lg} = v_{cf}^* - V_g \tag{8}$$

$$v_{cf}^* = V_g + \omega \cdot L_g \cdot I_{Lg}^*. \tag{9}$$

From (9), the required capacitor voltage for regulating the grid-side current can be calculated by *d-q* transformation as follows:

$$\begin{pmatrix} v_{cf}^{d^*} \\ v_{cf}^{q^*} \end{pmatrix} = \begin{pmatrix} V_g^d \\ 0 \end{pmatrix} + \omega L_g \begin{pmatrix} i_{Lg}^{q^*} \\ -i_{Lg}^{d^*} \end{pmatrix} \tag{10}$$

where V_g^d is the peak of the grid voltage, and V_g^q is *q* component of the grid voltage V_g and equal to zero by the phase synchronization. Equation (10) is shown in the i_{Lg} control block of

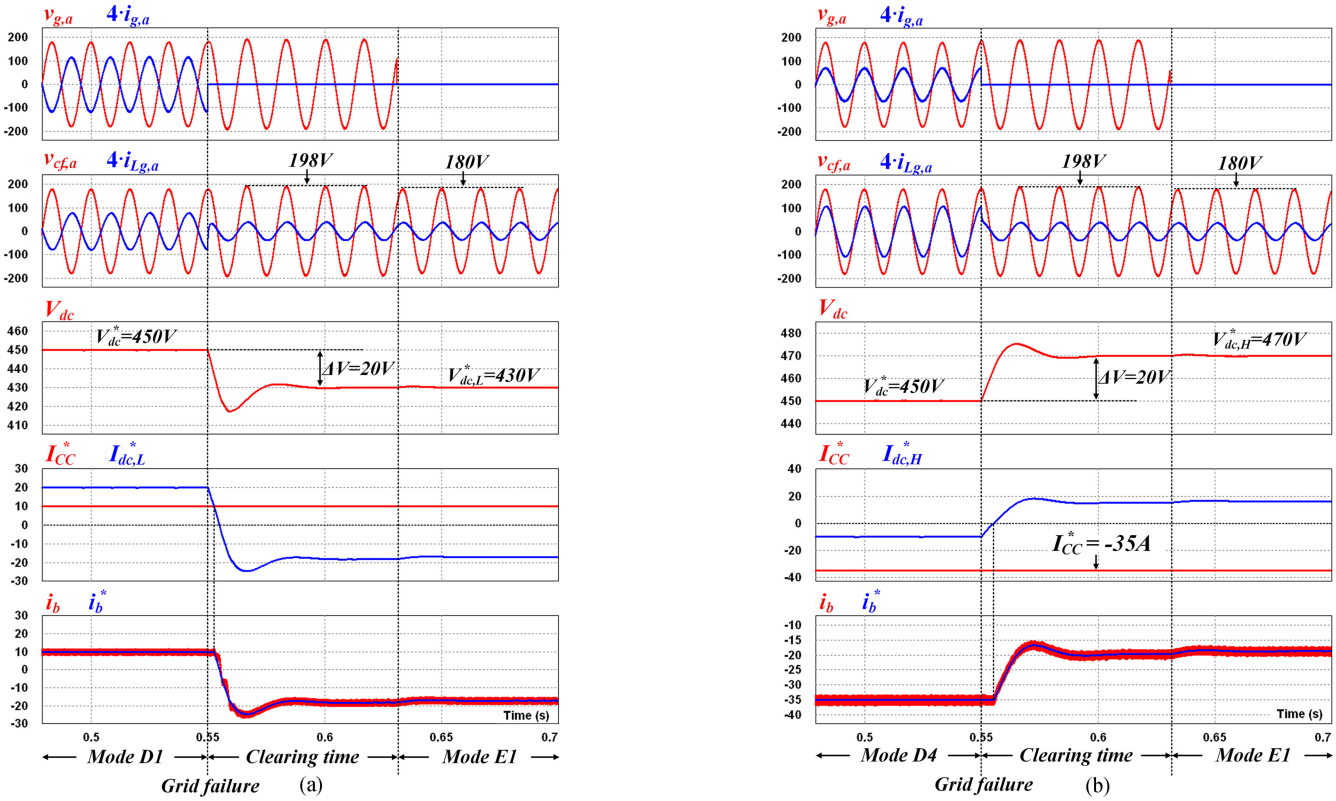

Fig. 10. Simulation waveforms of the proposed hybrid ESS-UPS showing the mode change. (a) Mode D1 to Mode E1. (b) Mode D4 to Mode E1.

Fig. 9, and the three-level ac–dc converter controls the grid-side current by controlling the capacitor voltage based on (10).

When the grid fails, the three-level ac–dc converter operates in emergency power supply mode, and the i_{Lg} controllers are saturated and their outputs are restricted by the limiters. It is note that the limiter's outputs are limited to 10% of the nominal grid voltage in this paper, and therefore the VFD load voltage is controlled within the normal operating voltage range during the islanding detection period. Then, the capacitor voltage reference is determined as follows:

$$\begin{pmatrix} v_{cf}^{d*} \\ v_{cf}^{q*} \end{pmatrix} = \begin{pmatrix} V_g^d \\ 0 \end{pmatrix}. \tag{11}$$

In emergency power supply mode, the three-level ac–dc converter regulates the capacitor voltage to the same magnitude of the grid voltage so that it is capable of supplying emergency power to the VFD load. Note that there is a small variation (10% of the nominal value) in v_{cf}^{d*} and the control parameters of the v_{cf} controllers do not change at the mode change. Therefore, the proposed control can provide the VFD load with a stable voltage during the clearing time and achieve seamless mode transfer.

IV. Simulation Results

Fig. 10(a) and (b) shows the simulation waveforms of the mode change from Mode D1 to Mode E1 and Mode D4 to Mode E1, respectively, when the grid fails. In the simulation, the nominal dc-link voltage is set to 450 V, and battery charging current reference and battery discharging current reference are set to 10 and –35 A, respectively. In Mode D1 of Fig. 10(a),

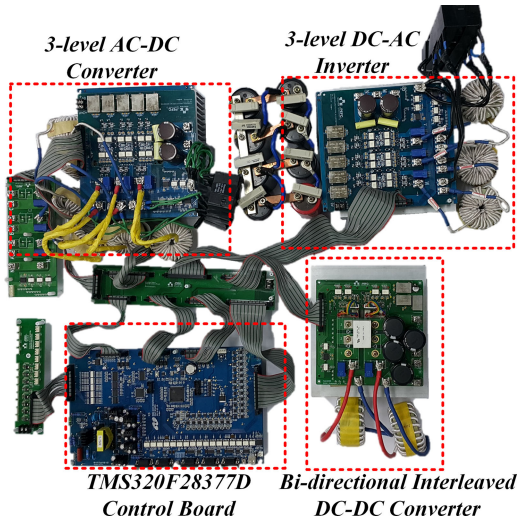

Fig. 11. Photograph of the 5-kW prototype.

the ac–dc converter is regulating the dc-link voltage to 450 V while the dc–dc converter is charging the battery with 10 A. When the grid fails, the ac–dc converter changes the control objectives and starts to regulate the VFD load voltage, contributing to drop of the dc-link voltage. A decrease of the dc-link voltage activates PI_3, shown in Fig. 8, and the dc–dc converter starts to regulate the dc-link voltage to 430 V after $I_{\mathrm{dc},L}{}^{*}$ becomes smaller than 10 A. In Mode D4 of Fig. 10(b), the ac–dc converter is regulating the dc-link voltage to 450 V while the dc–dc converter is discharging the battery with –35 A. When the grid

TABLE IV
SYSTEM PARAMETERS OF THE PROPOSED HYBRID ESS-UPS

ac-dc converter			dc-ac inverter			dc-dc converter		
Symbol	Value	Unit	Symbol	Value	Unit	Symbol	Value	Unit
P	5	kW	P	5	kW	P	5	kW
V_g	220	V_{ac}	f_{sw}	10.8	kHz	f_{sw}	10.8	kHz
f_{sw}	10.8	kHz	V_{ci}	220	V_{ac}	V_b	210~310	V_{dc}
V_{dc}	430~470	V_{dc}	L_i	540	μH	L_1, L_2	1.17	mH
L_g	560	μH	C_i	16	μF	C_o	165	μF
L_f	540	μH	$C_{dc,P}$, $C_{dc,N}$	6	mF			
C_f	16	μF						

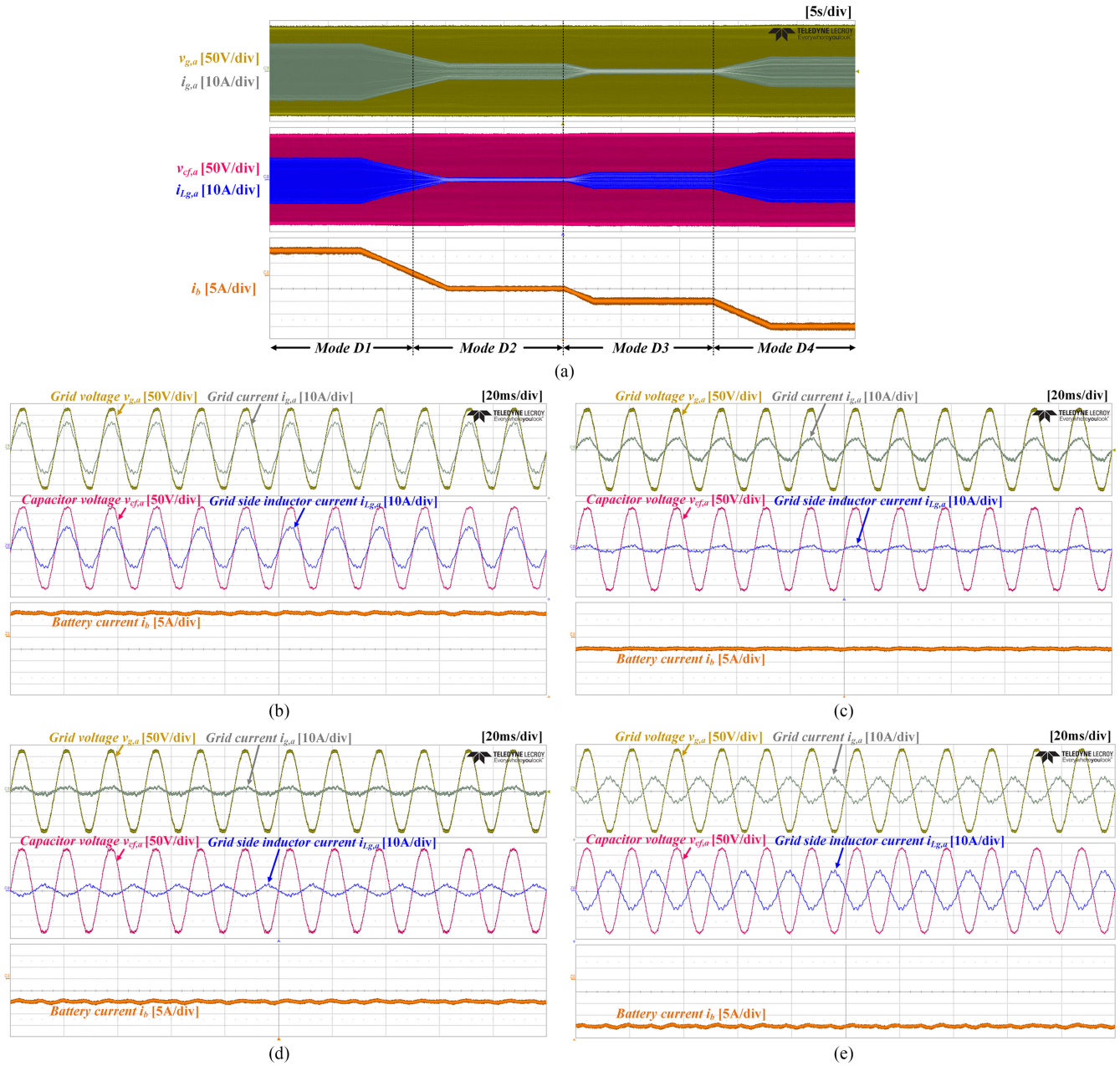

Fig. 12. Experimental waveforms of mode change. (a) Mode D1 to Mode D4. (b) Zoomed-in waveform of Mode D1. (c) Zoomed-in waveform of Mode D2. (d) Zoomed-in waveform of Mode D3. (e) Zoomed-in waveform of Mode D4.

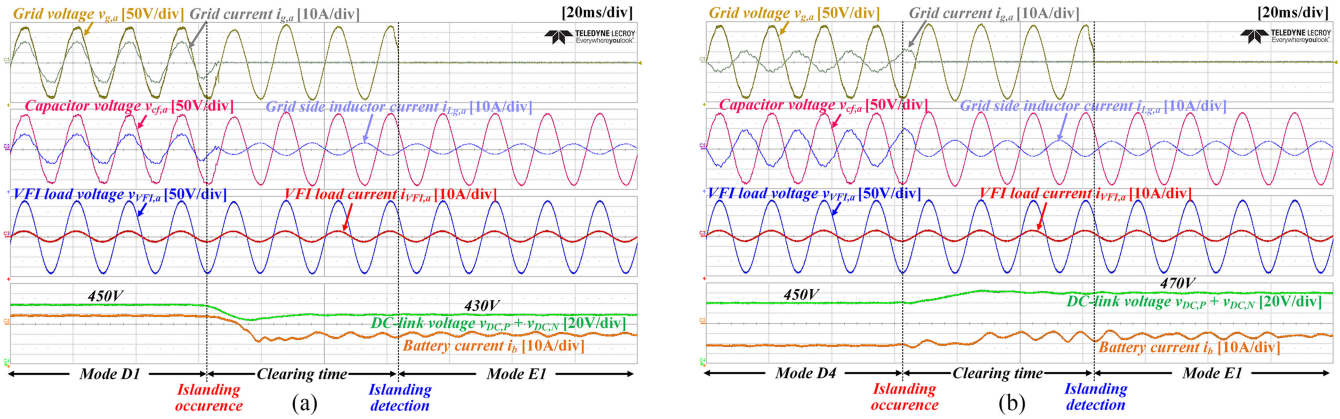

Fig. 13. Experimental waveforms of mode change. (a) Mode D1 to Mode E1. (b) Mode D4 to Mode E1.

fails, the ac–dc converter changes the control objectives and starts to regulate the VFD load voltage, contributing to increase of the dc-link voltage. An increase in the dc-link voltage activates PI_1, and the dc–dc converter starts to regulate the dc-link voltage to 470 V after $I_{dc,H}{}^*$ becomes greater than 0 A. The simulation results show that the ac–dc converter changes the mode from the dc-link voltage control mode to the VFD load voltage control mode without any transients across the VFD load voltage, and the dc–dc converter autonomously changes the mode from the battery current control mode to the dc-link voltage control mode.

V. Experimental Results

Fig. 11 shows a photograph of a 5-kW prototype of the proposed hybrid ESS-UPS that is composed of the three-level ac–dc converter, the three-level dc–ac inverter, and the bidirectional dc–dc converter. The control algorithm was implemented by means of a dual core DSP TMS320F28377D. The system parameters of the proposed hybrid ESS-UPS are listed in Table IV.

Fig. 12(a) shows the four demand management modes of the proposed hybrid ESS-UPS that represent Mode D1, Mode D2, Mode D3, and Mode D4. Fig. 12(b)–(e) is zoomed-in waveforms of Fig. 12(a). Fig. 12(b) shows Mode D1, the battery charging mode. It can be seen that the battery current is positive, and the grid current and the grid-side inductor current are in phase with the grid voltage. Fig. 12(c) shows Mode D2, the battery discharging mode, and it can be seen that the battery current direction is negative, which means that the VFI load power is supplied by the grid and the battery. In Mode D3, as shown in Fig. 12(d), the battery discharging power is supplied to the VFI load, and the VFD load power is supplied by the grid and the battery. In Mode D4, as shown in Fig. 12(e), the battery discharging power is supplied to the VFI load and the VFD load, and the rest of the battery discharging power is injected to the grid.

Fig. 13(a) and (b) shows the experimental results of mode change from Mode D1 to Mode E1 and from Mode D4 to Mode E1, respectively, when the grid fails. In Fig. 13(a), when the system is in battery charging mode (Mode D1), the dc-link voltage is regulated by the ac–dc converter to 450 V, and the battery is charged by the bidirectional dc–dc converter. Thereafter, when the grid fails, the dc–dc converter takes over responsibility for dc-link voltage regulation from the ac–dc converter, and the ac–dc converter starts to regulate the voltage of the VFD load. Then, the dc-link voltage is reduced to 430 V because the grid fails during battery charging. Note that the VFD load does not have any transients. In Fig. 13(b), in the same way, when the system is in battery discharging mode (Mode D4), the dc-link voltage is regulated by the ac–dc converter to 450 V, and the battery is charged by the dc–dc converter. Thereafter, when the grid fails, the dc–dc converter takes over responsibility of dc-link voltage regulation from the ac–dc converter, and the ac–dc converter starts to regulate the voltage of the VFD load. Then, the dc-link voltage increases to 470 V because the grid fails during battery discharging. Note that the VFD load does not have any transients.

VI. Conclusion

This study proposes a hybrid ESS-UPS having demand management and emergency power supply functions. The proposed system achieves PCS cost reduction by integrating a PCS for ESSs with that of a UPS. In addition, the proposed system increases the capacity of emergency power supply by supplying the VFD load as well as the VFI load when the grid fails. The proposed system also increases the battery utilization by using the battery energy for not only demand management, but also emergency power supply. The operation modes of the hybrid ESS-UPS are introduced, and the fast mode transfer algorithm is proposed to alleviate transients during mode transfer. Experimental results from a 5-kW prototype are presented to validate the concept of the proposed operating modes and seamless mode transfer algorithm.

References

[1] S. M. Amin, "Smart grid overview issues and opportunities. Advances and challenges in sensing modeling simulation optimization and control," *Eur. J. Control*, vol. 17, no. 5-6, pp. 547–567, 2011.
[2] S. M. Amin, "North America's electricity infrastructure: are we ready for more perfect storms?," *IEEE Security Privacy*, vol. 1, no. 5, pp. 19–25, Sep./Oct. 2003.
[3] California ISO, Summer Loads & Resources Assessment, Infrastructure Development, California ISO, Folsom, CA, USA, 2015. [Online]. Available: http://www.caiso.com/Documents/2015SummerAssessment.pdf
[4] C. Klinger, O. Landeg, and V. Murray, Power outages, extreme events and health: A systematic review of the literature from 2011–2012, *Plos. Current Disasters*, vol. 1, Jan. 2014.
[5] S. M. Amin, "Security challenges for the electricity infrastructure," *Computer*, vol. 35, no. 4, pp. 8–10, Apr. 2002.

[6] Australian Energy Market Operator, Melbourne, VIC, Australia, Deferred 2015 Electricity Statement of Opportunities for the WEM. 2016. [Online]. Available: https://www.aemo.com.au/Electricity/Wholesale-Electricity-Market-WEM/Planning-and-forecasting/WEM-Electricity-Statement-of-Opportunities
[7] G. Wang *et al.*, "A review of power electronics for grid connection of utility-scale battery energy storage systems," *IEEE Trans. Sustain. Energy*, vol. 7, no. 4, pp. 1778–90, Jul. 2016.
[8] X. Tan, Q. Li, and H. Wanga, "Advances and trends of energy storage technology in microgrid," *Int. J. Elect. Power Energy Syst.*, vol. 44, pp. 179–191, 2013.
[9] C. N. K. Nair and G. Niraj, "Battery energy storage systems: Assessment for small-scale renewable energy integration," *Energy Build.*, vol. 42, no. 11, pp. 2124–2130, 2010.
[10] T. Kousksou, "Energy storage: Applications and challenges," *Solar Energy Mater. Solar Cells*, vol. 120, Part. A, pp. 59–80, Jan. 2014.
[11] J. Leadbetter and L. Swan, "Battery storage system for residential electricity peak demand shaving," *Energy Build.*, vol. 55, pp. 685–692, Dec. 2012.
[12] S. Vazquez, S. M. Lukic, E. Galvan, L. G. Franquelo, and J. M. Carrasco, "Energy storage systems for transport and grid applications," *IEEE Trans. Ind. Electron.*, vol. 57, no. 12, pp. 3881–3895, Dec. 2010.
[13] H. Kuniyoshi, "Power grid electrical energy storage," Glob. Smart Grid Fed. (GSGF), Japan, Jan. 2016.
[14] U.S. Department of Energy, "Analysis insights: Energy storage—possibilities for expanding electric grid flexibility," Nat. Renewable Energy Lab., 2016. [Online]. Available: http://www.nrel.gov/docs/fy16osti/64764.pdf
[15] U.S. Department of Energy, "Maintaining reliability in the mordern power system," Energy Policy Syst. Anal. office, U.S. Dept. Energy, 2016. [Online]. Available: https://energy.gov/epsa/downloads/maintaining-reliability-modern-power-system
[16] K. Popper and A. Hove, "Energy storage world markets: 2014-2020," presented at the *2017 Energy Storage World Forum*, Berlin, Germany, May 2017.
[17] F. Hina and K. Palanisamy, "Energy storage systems for energy management of renewables in distributed generation systems," in *Energy Management of Distributed Generation Systems*. Rijeka, Croatia: InTech, 2016.
[18] D. Zhu, S. Yue, N. Chang, and M. Pedram, "Toward a profitable grid-connected hybrid electrical energy storage system for residential use," *IEEE Trans. Comput.-Aided Des. Integr. Circuits Syst.*, vol. 35, no. 7, pp. 1151–1164, Jul. 2016.
[19] A. C. Luna, N. L. Diaz, M. Graells, J. C. Vasquez, and J. M. Guerrero, "Online energy management system for distributed generators in a grid connected microgrid," in *Proc. IEEE Energy Convers. Congr. Expo.*, 2015, pp. 4616–4623.
[20] F. Kazhamiaka, C. Rosenberg, and S. Keshav, "Practical strategies storage operation in energy systems: Design and evaluation," *IEEE Trans. Comput.-Aided Des. Integr. Circuits Syst.*, vol. 35, no. 7, pp. 1602–1610, Jul. 2016.
[21] M. A. Abusara, J. M. Guerrero, and S. M. Sharkh, "Line-interactive ups for microgrids," *IEEE Trans. Ind. Electron.*, vol. 61, no. 3, pp. 1292–1300, Mar. 2014.
[22] B. Zhao, Q. Song, W. Liu, and Y. Xiao, "Next-generation multi-functional modular intelligent UPS system for smart grid," *IEEE Trans. Ind. Electron.*, vol. 60, no. 9, pp. 3602–3618, Sep. 2013.
[23] E. H. Kim, J. M. Kwon, J. K. Park, and B. H .Kwon, "Practical control implementation of a three- to single-phase online UPS," *IEEE Trans. Ind. Electron.*, vol. 55, no. 8, pp. 2933–2942, Aug. 2008.
[24] J. M. Guerrero, L. G. de Vicuna, and J. Uceda, "Uninterruptible power supply systems provide protection," *IEEE Ind. Electron. Mag.*, vol. 1, no. 1, pp. 28–38, May 2007.
[25] R. Krishnan and S. Srinivasan, "Topologies for uninterruptible power supplies," in *Proc. IEEE Int. Symp. Ind. Electron.*, Budapest, Hungary, 1993, pp. 122–127.
[26] D. I. W. Sölter, "An international UPS classification by IEC 62040-3," in *Proc. 24th Annu. Int. Telecommun. Energy Conf.*, Sep. 2002, pp. 541–545.
[27] G. Albright, J. Edie, and S. Al-Hallaj, "A comparison of lead acid to lithium-ion in stationary storage applications," Allcell Technologies LLC, Chicago, IL, USA, White Paper, 2012.
[28] S. Jung, R. Bernardino, and C. Gonjin, "Lithium ion battery system in data centers," in *Proc. 2015 Int. Conf. Environ. Elect. Eng.*, 2015, pp. 968–973.
[29] G9000 Uninterruptible Power Supply Multi-level PWM IGBT Technology (UPSG9000WP081201, Toshiba International Corporation, Houston, TX, USA, 2008.
[30] J. Park and S. Choi, "Design and control of a bidirectional resonant dc–dc converter for automotive engine/battery hybrid power generators," *IEEE Trans. Power Electron.*, vol. 29, no. 7, pp. 3748–3757, Jul. 2014.
[31] M. Kwon, J. Park, and S. Choi, "Design and control strategy for autonomous and seamless mode transition of high efficiency bidirectional DC-DC converter for ISG systems," *Trans. Korean Inst. Power Electron.*, vol. 21, no. 1, pp. 19–26, Feb. 2014.
[32] S. Choi, J. Park, and M. Kwon, "System for controlling bidirectional converter," Korean Patent 10-1417669, Jul. 2, 2014.
[33] J. Schonberger, R. Duke, and S. D. Round, "DC-Bus signaling: A distributed control strategy for a hybrid renewable nanogrid," *IEEE Trans. Ind. Electron.*, vol. 53, no. 5, pp. 1453–1460, Oct. 2006.
[34] K. Sun, L. Zhang, Y. Xing, and J. M. Guerrero, "A distributed control strategy based on DC bus signaling for modular photovoltaic generation systems with battery energy storage," *IEEE Trans. Power Electron.*, vol. 26, no. 10, pp. 3032–3045, Oct. 2011.
[35] C. Bohn and D. P. Atherton, "An analysis package comparing PID anti-windup strategies," *IEEE Control Syst. Mag.*, vol. 15, no. 2, pp. 34–40, Apr. 1995.
[36] H. Kim, T. Yu, and S. Choi, "Indirect current control algorithm for utility interactive inverters in distributed generation systems," *IEEE Trans. Power Electron.*, vol. 23, no. 3, pp. 1342–1347, May 2008.
[37] J. Kwon, S. Yoon, and S. Choi, "Indirect current control for seamless transfer of three-phase utility interactive inverters," *IEEE Trans. Power Electron.*, vol. 27, no. 2, pp. 773–781, Feb. 2012.
[38] S. Choi and S. Yoon, "Utility interactive inverter of three phase-indirect current control type and control method," Korean Patent 10-1178393, Aug. 24, 2012.

Sangjin Kim was born in Korea, in 1988. He received the B.S. and M.S. degrees in control and instrumentation engineering from Seoul National University of Science and Technology (Seoul Tech), Seoul, South Korea, in 2015 and 2017, respectively, where he is currently working toward the Ph.D. degree in electrical and information engineering, Seoul Tech.

His research interests include bidirectional dc–dc converter and three-phase grid-connected inverter for uninterruptible power supplies, and energy storage systems.

Minho Kwon was born in Korea, in 1985. He received the B.S. and M.S. degrees in control and instrumentation engineering from Seoul National University of Science and Technology (Seoul Tech), Seoul, South Korea, in 2012 and 2014, respectively, where he is currently working toward the Ph.D. degree in electrical and information engineering, Seoul Tech.

His research interests include bidirectional dc–dc converter and grid-connected inverter for electric vehicles and renewable energy systems.

Sewan Choi (S'92–M'96–SM'04) received the B.S. degree in electronic engineering from Inha University, Incheon, South Korea, in 1985, and the M.S. and Ph.D. degrees in electrical engineering from Texas A&M University, College Station, TX, USA, in 1992 and 1995, respectively.

From 1985 to 1990, he was with Daewoo Heavy Industries as a Research Engineer. From 1996 to 1997, he was a Principal Research Engineer at Samsung Electro-Mechanics Co., South Korea. In 1997, he joined the Department of Electrical and Information Engineering, Seoul National University of Science and Technology, Seoul, South Korea, where he is currently a Professor. His research interests include power conversion technologies for renewable energy systems and dc–dc converters and battery chargers for electric vehicles.

Prof. Choi is an Associate Editor of the IEEE TRANSACTIONS ON POWER ELECTRONICS and the IEEE JOURNAL ON EMERGING AND SELECTED TOPICS IN POWER ELECTRONICS.